Int. J. Environ. Sci. Technol. (2015) 12:1669–1676
DOI 10.1007/s13762-014-0533-z

ORIGINAL PAPER

Potential application of novel TiO_2/β-FeOOH composites for photocatalytic reduction of Cr(VI) with an analysis of statistical approach

M. Zhang · Z. Xu · J. Liang · L. Zhou · C. Zhang

Received: 5 August 2013 / Revised: 7 January 2014 / Accepted: 16 February 2014 / Published online: 9 April 2014

Abstract In this paper, four TiO_2/β-FeOOH photocatalysts were synthesized by a simple deposition–precipitation method and characterized by X-ray diffraction, fourier transform infrared, scanning electron microscope and transmission electron microscope. The characterization showed the presence of nano-sized β-FeOOH particles on the TiO_2 support. The photocatalytic efficiency of the catalysts was examined on the Cr(VI) reduction under ultraviolet irradiation in aqueous suspension. The photocatalyst denoted as 25TiO_2/β-FeOOH appeared to be most efficient, which is due to effectively inhibiting the recombination of photoinduced electrons and holes. A 2^4 factorial design methodology was employed to evaluate the statistically important operating conditions (pH of the solution, loading of catalyst, Cr(VI) concentration and reaction time) and their interactions on the photocatalytic reduction efficiency of Cr(VI) over 25TiO_2/β-FeOOH.

Keywords Chromium reduction · Photocatalysis · TiO_2/β-FeOOH · Composites · Factorial design

Introduction

Hexavalent chromium is toxic and mobile, causing particular environmental concern. Thus, it is essential to be removed from industrial wastewater (Barrera-Díaz et al. 2012). A strong oxidizing agent, hexavalent chromium is carcinogenic and mutagenic and diffuses quickly through soil and aquatic environments. The most probable Cr(VI) species in aqueous solution are $Cr_2O_7^{2-}$, CrO_4^{2-}, H_2CrO_4, and $HCrO_4^-$, the relative distribution of which depends on the solution pH, Cr(VI) concentration and redox potential (Cespón-Romero et al. 1996). However, none of these Cr(VI) species form insoluble precipitates making its separation impossible with a direct precipitation method (Nriagu and Nieboer 1988), whereas Cr (III), being less toxic and mobile, can be readily precipitated out of solution in the form of $Cr(OH)_3$ (Eary and Rai 1988; Yurik and Pikaev 1999). To remove Cr(VI) from the aqueous media, it is necessary to reduce Cr(VI) to Cr(III) first (Olmez 2009; Singh et al. 2011).

Recently, the photocatalytic reduction of hexavalent chromium in aqueous solutions using semiconductor particles has been widely studied (Ku and Jung 2001; Jiang et al. 2006; Yoon et al. 2009). The strong interest in TiO_2 lies in the fact that it is non-toxic, inexpensive, highly photoactive, harmless, and easily synthesized and handled. However, electron transfer and the recombination between electron–hole pairs results in low quantum yields for most photocatalytic reactions (Rengaraj et al. 2007; Parida and Sahu 2008; Qiu et al. 2012). The application of coupled semiconductors in the photocatalytic process is regarded as an alternative to enhance the photocatalytic activity of TiO_2 by inhibiting the recombination of electron–hole pairs (Pal et al. 1999; Fresno et al. 2008; Banić et al. 2011; Sun et al. 2012; Yu et al. 2013). Fe_2O_3 is considered to be a suitable semiconductor to be coupled with TiO_2 due to its high photocatalytic activity and approximate band gap energy as compared with TiO_2 (Pal et al. 1999; Banić et al. 2011; Sun et al. 2012; Yu et al. 2013). Fe_2O_3 can be prepared by the forced hydrolysis of Fe^3 solutions. Iron

M. Zhang · J. Liang · L. Zhou
Department of Environmental Engineering, College of Resources and Environmental Sciences, Nanjing Agricultural University, Nanjing 210095, People's Republic of China

Z. Xu (✉) · C. Zhang
Department of Chemistry, College of Science, Nanjing Agricultural University, Nanjing 210095, People's Republic of China
e-mail: xuzhihui@njau.edu.cn

oxyhydroxides (α-FeOOH and β-FeOOH) are intermediate products and can transform to Fe_2O_3 through the dissolution/recrystallization process (Sugimoto and Muramatsu 1996; Liu et al. 2005; Liang et al. 2006; Štajdohar et al. 2012). Akaganéite (β-FeOOH) has a channel structure parallel to the c-axis (Yuan et al. 2004). This tunnel structure makes β-FeOOH an especially interesting material as promising photo-Fenton catalyst in the heterogeneous system (Benz et al. 1998; Zhao et al. 2010). Based on these literatures, we are motivated to work in this direction and engage in fabricating TiO_2/β-FeOOH composite photocatalysts with various TiO_2 dosages by wetness impregnation method. Herein, for the first time, we report the modification of TiO_2 (P25) by β-FeOOH nanoparticles as a composite photocatalyst, which exhibits excellent photocatalytic activity for the reduction of Cr(VI). All the experiments had been completed at Nanjing Agriculture University by the end of June 30, 2013.

Materials and methods

Catalyst preparation

All the chemicals were of analytical grade and used without further purification. All glasswares were cleaned by soaking in 1 M HCl for 12 h and thoroughly rinsed with tap water and then deionized water.

Four TiO_2/β-FeOOH materials, with the different content of TiO_2, were obtained by deposition–precipitation method; 10.8116 g $FeCl_3 \cdot 6H_2O$ was added to a solution of 2.4000 g urea in 100 ml deionized water under permanent magnetic stirring for 30 min. Without adjusting the pH value, the required mass of TiO_2 (Degussa P25) was added to the above mixed solution. After additional stirring for 24 h, the obtained suspension was transferred into a Teflon-lined stainless steel autoclave (200 ml). The sealed autoclave was maintained at 90 °C for 8 h, and then cooled to room temperature naturally. The resulting sample was collected by centrifugation, washed several times with absolute ethanol and deionized water, and finally dried at 60 °C for 24 h. By applying this procedure, 4 samples with the TiO_2/Fe^3 mole ratio of 10:90, 25:75, 40:60, and 50:50 in the initial suspensions (denoted as $10TiO_2$/β-FeOOH, $25TiO_2$/β-FeOOH, $40TiO_2$/β-FeOOH, and $50TiO_2$/β-FeOOH) were prepared. The sample obtained by the same procedure but without addition of TiO_2 was denoted as β-FeOOH.

Catalyst characterization

The powder X-ray diffraction (XRD) patterns were recorded at a scanning rate of 4° min^{-1} in the 2θ range of 10°–80° using a Bruker D8 Advance instrument with Cu–Kα radiation ($\lambda = 1.5406$ □) at room temperature. The morphologies and nanostructures of synthesized products were further observed using a Hitachi S-3400N scanning electron microscope (SEM) at the acceleration voltage of 20 kV and a Hitachi H-7650 transmission electron microscope (TEM) at the acceleration voltage of 80 kV. Fourier transform infrared (FT-IR) spectrum measurements were performed on a Bruker Vector 22 FT-IR spectrophotometer, with scanning from 4,000 to 400 cm^{-1} using KBr pellets.

Photocatalytic reduction of Cr(VI)

$K_2Cr_2O_7$, used as a source of hexavalent chromium, was dried at 120 °C for 2 h before weighing. A CyberScan pH2100 Bench Meter (Eutech Instruments), after three-point calibration, was applied to measure pH values. A phosphate buffer with a pH of 3.0 was prepared using H_3PO_4 and NaOH. The photocatalytic reduction of Cr(VI) was conducted in a XPA-7 photochemical reactor (Xujiang Electromechanical Plant, Nanjing, China) equipped with a magnetic stirrer and a device controlling temperature. A 100-W medium pressure Hg lamp as a source of ultraviolet (UV) light was positioned inside a cylindrical Pyrex vessel surrounded by a circulating water Pyrex jacket to cool the lamp.

For typical photocatalytic runs, TiO_2/β-FeOOH composite catalysts (0.01 g) were suspended in 50 mL aqueous solution of potassium dichromate buffered by phosphate. The initial concentrations of Cr(VI) and phosphate were 100 μM and 0.01 M, respectively. Prior to illumination, the suspension was first magnetically stirred in dark for 30 min to ensure the establishment of adsorption–desorption equilibrium on catalyst surface so that the loss of Cr(VI) was taken into account due to adsorption. The reaction mixture was maintained at 25 ± 1 °C by a magnetic stirrer at 600 rpm before and during the irradiation. The temperature of the reaction suspension was maintained by cooling water circulation. At appropriate time intervals, approximately 2 mL sample was drawn out from the quartz tube using a syringe and immediately filtered through a 0.45-μm filter membrane to remove catalyst. Finally, 1 ml aliquot of the filtrate was utilized for Cr(VI) analysis.

Analysis of Cr(VI) concentration

The developer, 1, 5-diphenylcarbazide (DPC), was purchased from Sigma-Aldrich, and its stock solution was kept in a refrigerator in a brown bottle prior to use. Cr(VI) concentration was determined by DPC colorimetric method, using a dilute sulfuric acid solution (pH 2.0) to control pH for the color development. The absorbance was measured in a 1-cm cell at 540 nm on a UV-9100 Spectrophotometer (Beijing Ruili Corp.). The reduction efficiency of Cr(VI) was calculated with the following formula:

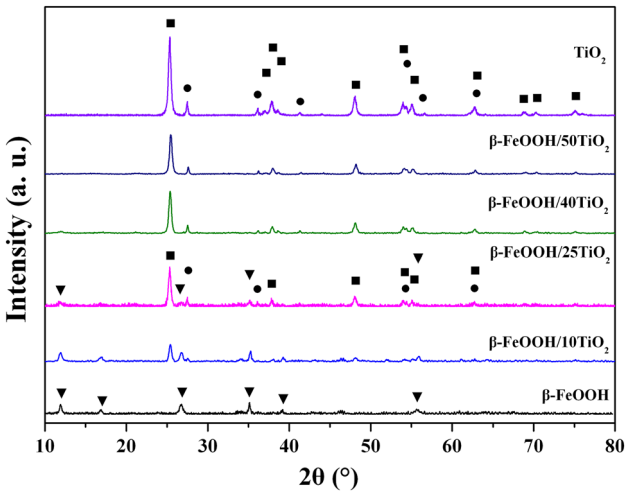

Fig. 1 XRD patterns of TiO_2, β-FeOOH, and TiO_2/β-FeOOH composites (*filled square* Anatase; *filled circle* Rutile; *filled inverted triangle* Pure β-FeOOH)

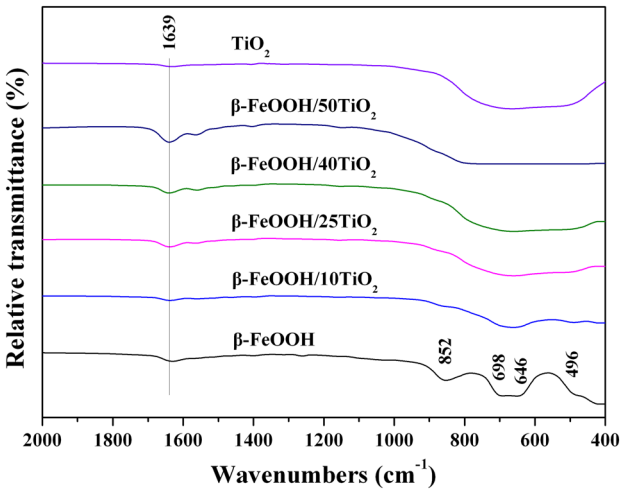

Fig. 2 Characteristic parts of the FT-IR spectra of TiO_2, β-FeOOH and TiO_2/β-FeOOH composites

$$\eta_R = \frac{(C_0 - C_t)}{C_0} \times 100\,\% \quad (1)$$

Where η_R is the reduction efficiency of Cr(VI), C_0 and C_t are the concentration of Cr(VI) solution at initial time and after irradiated at t time, respectively.

Results and discussion

Structural characteristics of prepared photocatalysts

Figure 1 exhibits the X-ray diffraction patterns of TiO_2 (Degussa P25), β-FeOOH, and $25TiO_2$/β-FeOOH photocatalysts. The XRD pattern of the β-FeOOH sample matched the diffraction of tetragonal pure β-FeOOH (JCPDS card No. 34-1266) very well with cell constants of $a_0 = 10.51$ Å, $b_0 = 10.51$ Å, and $c_0 = 3.033$ Å, and no impurity peak can be detected. It is known that Degussa P25, considered as one of the best photocatalyst, is a mixture (Konlen'ko et al. 2004). As shown in Fig. 1, the diffraction peaks at 2θ of 25.28°, 36.98°, 37.80°, 38.58°, 48.02°, 53.89°, 55.06°, 62.69°, 68.76°, 70.31°, and 75.03° can be indexed to the characteristic peaks (101), (103), (004), (112), (200), (105), (211), (204), (116), (220), and (215) of anatase (JCPDS card No. 21-1272), respectively. Whereas, the other diffraction peaks of TiO_2 sample can be indexed to the characteristic peaks of rutile (JCPDS card No. 21-1276). For the samples of $10TiO_2$/β-FeOOH and $25TiO_2$/β-FeOOH, several small peaks located at 2θ values of 11.84°, 26.72°, 35.16°, and 55.90° suggest the appearance of β-FeOOH phase, which was mixed with the anatase TiO_2 phase and rutile TiO_2 phase. In addition, negligible changes of all diffraction peak positions of anatase and rutile phase TiO_2 compared with that of the TiO_2 sample suggest that Fe^3 does not incorporate into the lattice of TiO_2, but as β-FeOOH deposits on the surface of TiO_2. Furthermore, it can be observed that the diffraction peaks of β-FeOOH phase become slightly broader, which indicates that the β-FeOOH particle size reduces. This result will be further tested and verified by SEM and TEM observation. However, the diffraction peaks of β-FeOOH phase almost disappeared in the $40TiO_2$/β-FeOOH and $50TiO_2$/β-FeOOH samples, which suggests that excess of TiO_2 is not conducive to the formation of β-FeOOH crystalline.

The photocatalysts were analyzed by FT-IR spectrophotometer for further identification. As shown in Fig. 2, the absorption peak at wavelength 1,639 cm^{-1} was attributed to the O–H vibrations of absorbed H_2O molecules or structural OH groups (Cheng and Zhao 2011; Tong et al. 2011). The wide band between 1,000 and 400 cm^{-1} of TiO_2 sample was aroused by stretching vibration of Ti–O (Wang et al. 2006). For the catalyst of β-FeOOH, the absorption peaks at wavelength 852, 698, 646, and 496 cm^{-1} were assigned to the vibration modes of the FeO_6 coordination octahedron (Ristic et al. 2005; Cheng and Zhao 2011). Compared with FT-IR spectra of $10TiO_2$/β-FeOOH, $25TiO_2$/β-FeOOH, $40TiO_2$/β-FeOOH, and $50TiO_2$/β-FeOOH, the most interesting point is probably that the absorption peaks at wavelength 852, 698, 646, and 496 cm^{-1} gradually weakens and almost completely disappeared with the increase in TiO_2/Fe^3 mole ratio of in the initial suspensions. This phenomenon indicates that β-FeOOH was not simply to cover the surface of TiO_2, but likely to form the strong interaction (such as Fe–O–Ti bond) with TiO_2 (Li et al. 2009).

Figure 3a–c shows the SEM images of TiO_2, β-FeOOH, and $25TiO_2$/β-FeOOH catalysts, respectively. It demonstrates that TiO_2 is characterized by a single morphology with approximately globular structure and loose agglomeration. The observed average particles' diameter of the

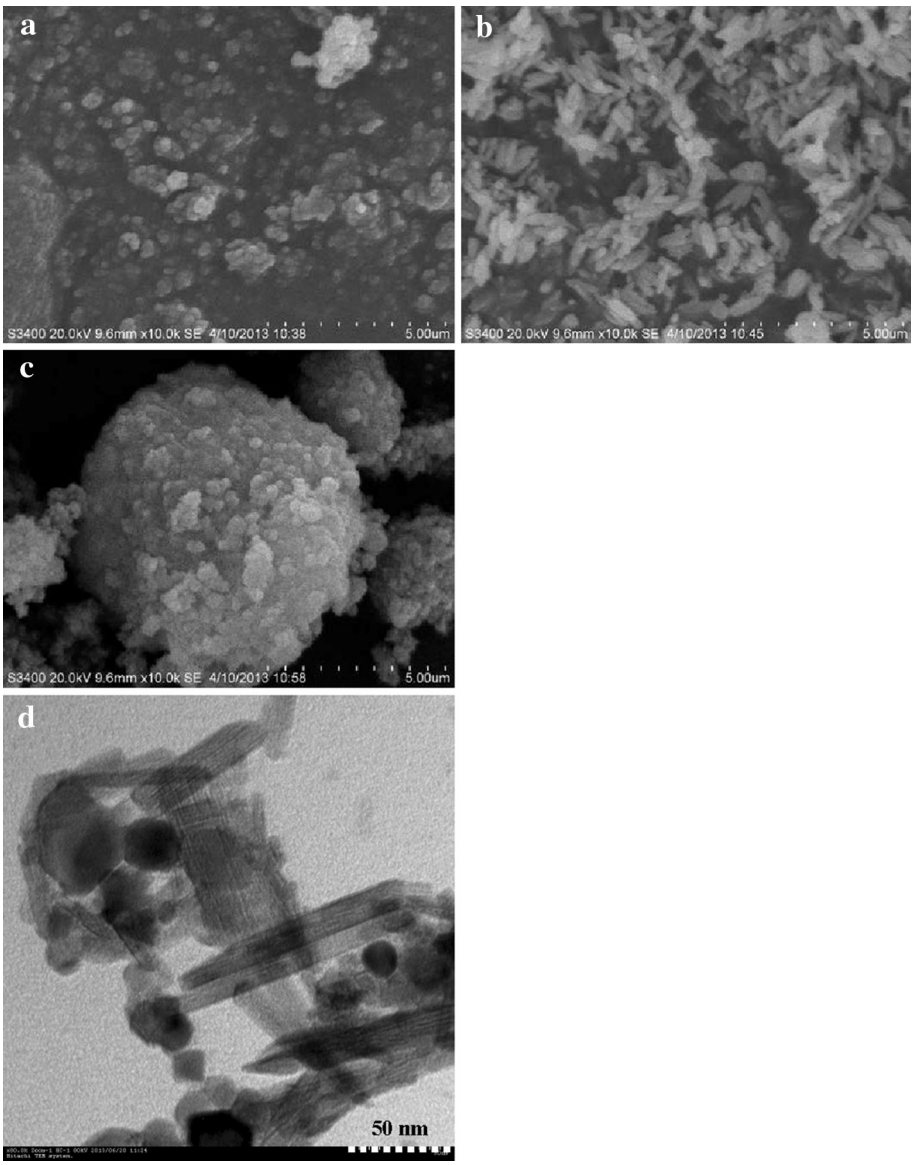

Fig. 3 SEM images of different catalysts (**a** TiO_2; **b** β-FeOOH; **c** $25TiO_2$/β-FeOOH; the whole *scale bar* is 5 μm) and TEM image of $25TiO_2$/β-FeOOH (**d** the whole *scale bar* is 50 nm)

TiO_2 sample is about 0.24 μm. β-FeOOH catalyst exhibits shuttle-like shape with an average width of about 0.25 μm and length of about 0.86 μm. However, the $25TiO_2$/β-FeOOH composite shows nest-like morphology with diameter range from 2 μm to more than 12 μm. It is clearly shown that smaller short-rod-like particles cover the surface of the nested structure. Based on the above discussion, the smaller short-rod-like particles should be β-FeOOH particles whose average lengths are around 0.31 μm. During the synthesis of composite, the titanium dioxide nanoparticles served as heterogeneous nuclei for the growth of β-FeOOH, while the existence of TiO_2 nanoparticles also inhibited the growing up of β-FeOOH nanoparticles. It is in accordance with the XRD result. Further observation of the $25TiO_2$/β-FeOOH sample by TEM (Fig. 3d) reveals that the short rods of β-FeOOH nanoparticles are attached to the surface of TiO_2 nanoparticles.

Photocatalytic reduction of Cr(VI)

The temporal concentration variation of Cr(VI) by different photocatalysts is illustrated in Fig. 4. Eary and Rai (1991) observed that 0.01 M NaH_2PO_4 could effectively displace Cr (VI) species adsorbed on the soil surfaces. As shown in Fig. 4, only a little concentration decrease in Cr(VI) was observed during the test time in the presence of $25TiO_2$/β-FeOOH and the dark. Negligible concentration change of Cr(VI) was also observed in the dark reaction over other catalysts (data now shown), which suggests that the adsorption of Cr(VI) on catalysts surface in 0.1 M phosphate buffer can be ignored when investigating the photocatalytic reduction of Cr(VI).

In the presence of photocatalyst, Cr(VI) can be reduced to Cr(III) by the excited electrons initiated by UV irradiation. The overall reaction of Cr(VI) photoreduction could be described as follows (Jiang et al. 2006):

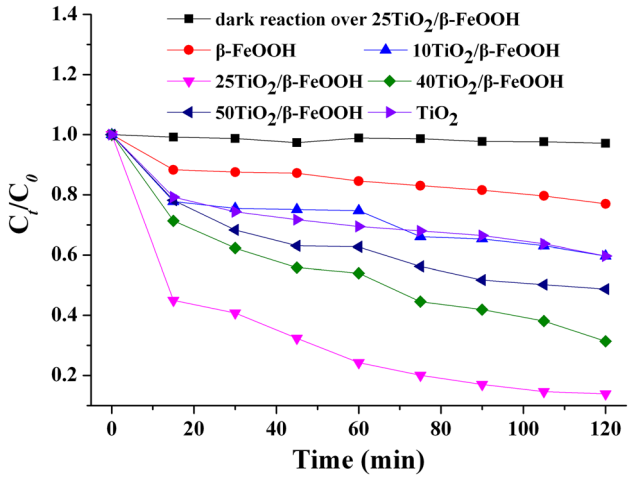

Fig. 4 Kinetics of photocatalytic reduction of Cr(VI) by TiO_2/β-FeOOH under UV light (100 W). Conditions: Cr(VI) concentration = 100 mg/L; pH 4.0; loading of catalyst = 0.010 g/50 mL

$$Cr_2O_7^{2-} + 14H^+ + 6e^- \rightarrow 2Cr^{3+} + 7H_2O \quad (2)$$

$$2H_2O + 4h^+ \rightarrow O_2 + 4H^+. \quad (3)$$

It was found that pseudo-first-order kinetics was obeyed for the photocatalytic reduction of Cr(VI). The calculated kinetics constants are listed in Table 1. All these catalysts were capable of reducing Cr(VI) in the order of β-FeOOH < TiO_2 ≈ 10TiO_2/β-FeOOH < 50TiO_2/β-FeOOH < 40TiO_2/β-FeOOH < 25TiO_2/β-FeOOH. The results reveal that the photocatalytic activity of β-FeOOH is lower than that of TiO_2 (P25) and TiO_2/β-FeOOH. Compared with β-FeOOH or TiO_2 catalyst, 25TiO_2/β-FeOOH composite catalyst significantly promoted the photocatalytic reduction of Cr(VI). The enhanced photocatalytic activity can be ascribed to the formation of TiO_2/β-FeOOH heterostructure, which plays an important role in the composite photocatalyst. When the 25TiO_2/β-FeOOH composite is under UV irradiation, electrons (e^-) are excited to the conduction band of β-FeOOH, leaving equal holes (h) in the valence band. Then holes will transfer from the valence band of β-FeOOH to that of TiO_2, the recombination of photoinduced carriers can be effectively inhibited, and thus can prolong the life time of photoinduced carriers. Consequently, the photocatalytic activity of 25TiO_2/β-FeOOH composite will be greatly improved.

Apart from the method of photocatalyst preparation, one of the key factors that governs the efficiency of composite photocatalyst is content of component in the heterostructure (Banić et al. 2011; Liu et al. 2012). The lower photocatalytic activity of the 10TiO_2/β-FeOOH composite can be ascribed to two main reasons. Firstly, during the preparation of the composite photocatalyst, β-FeOOH grew on the surface of TiO_2 and a core–shell heterostructure might form. At a low mole ratio of TiO_2/Fe^3 level, outer layer of β-FeOOH might grow too thick, and the photoinduced holes had to migrate over longer distance to the TiO_2 kernel. Secondly and more importantly, the higher contents Fe^3 ions in the composite catalyst played the role of recombination sites to trap the photoinduced electrons and holes (Banić et al. 2011), and thus decreased the photocatalytic efficiency of TiO_2/β-FeOOH catalyst. However, at a high mole ratio of TiO_2/Fe^3 level, the higher contents of TiO_2 in the composite catalysts might be not conducive to the formation of β-FeOOH crystalline structure, which leads to the low photocatalytic activity. Therefore, the photocatalytic activities of the 40TiO_2/β-FeOOH and 50TiO_2/β-FeOOH composites were also not high.

Table 1 Apparent kinetic values for the photocatalytic reduction of Cr(VI) by different catalysts

Name of the catalyst	Kinetic constant (min^{-1})	R^2 value
TiO_2	0.0014	0.8362
10TiO_2/β-FeOOH	0.0015	0.8544
25TiO_2/β-FeOOH	0.0065	0.9193
40TiO_2/β-FeOOH	0.0036	0.9576
50TiO_2/β-FeOOH	0.0024	0.9089
β-FeOOH	0.0007	0.8735

Analysis of operating conditions and their interactions on the Cr(VI) photocatalytic reduction efficiency by a statistical approach

In this study, a statistical approach was chosen based on a factorial experimental design that will allow us to infer about the effect of the operating conditions and their interactions on the Cr(VI) photocatalytic reduction efficiency with a relatively small number of experiments (Xu et al. 2013). Four factors in the experiment process, viz. pH of the solution, loading of catalyst (25TiO_2/β-FeOOH), Cr (VI) concentration and reaction time were taken into account as independent variables. As shown in Table 2, each variable receives two values, a high value (indicated by the sign) and a low value (indicated by the −sign). The experimental design followed in this work was a full 2^4 experimental set, which required 16 experiments. The 2^4 factorial experimental design matrix and the experimental results (response factor or dependent variable) obtained in photocatalytic reduction of Cr(VI) were presented in Table 3. Experimental data were analyzed by the use of Design-Expert 8.0.6 program.

In general, high levels of Cr(VI) reduction efficiency can be achieved at low pH of the reaction solution, low initial Cr(VI) concentration, high loading of catalyst, and long reaction time. The effect of solution pH on the conversion of Cr(VI) into Cr(III) is mainly ascribed to the

Table 2 Independent variables of the 2^4 factorial design of experiments

Level of value	X_1, pH	X_2, loading of catalyst (g/50 ml)	X_3, Cr(VI) concentration (μM)	X_4, reaction time (min)
−	4.0	0.01	100	15
+	5.0	0.02	300	60

Table 3 The 2^4 factorial experimental design matrix and the corresponding response factor (Y—photocatalytic reduction efficiency of Cr(VI))

Entry	X_1	X_2	X_3	X_4	Y (%)	
					Exp.[a]	Pred.[b]
1	−1	−1	−1	−1	54.98	56.51
2	1	−1	−1	−1	21.29	18.20
3	−1	1	−1	−1	72.04	69.46
4	1	1	−1	−1	30.52	31.15
5	−1	−1	1	−1	33.59	35.27
6	1	−1	1	−1	14.26	9.50
7	−1	1	1	−1	45.33	48.22
8	1	1	1	−1	18.75	22.45
9	−1	−1	−1	1	75.71	81.91
10	1	−1	−1	1	45.63	43.61
11	−1	1	−1	1	100.0	94.86
12	1	1	−1	1	52.08	56.56
13	−1	−1	1	1	59.97	60.67
14	1	−1	1	1	35.14	34.90
15	−1	1	1	1	78.90	73.62
16	1	1	1	1	46.55	47.85

[a]Experimental values of response

[b]Predicted values of response by the proposed model

enhanced chemical thermodynamic driving force for the reduction of Cr(VI). The lower the pH value of solution is, the higher the electrode potential of Cr(VI)/Cr(III) is, and thus accelerating the photocatalytic reduction of Cr(VI). In a hetero-catalytic reaction system, the catalytic reaction basically occurs on the surface of the catalyst. When at higher loading of catalyst, there will be more reactive centers in the photocatalytic reaction system and high levels of Cr(VI) reduction efficiency is achieved. As can be seen in Table 3, the highest Cr(VI) reduction efficiency of 100.0 % is obtained in entry 11.

According to the methodology of factorial design (Box et al. 1978), the estimation of the main effect, as well as the interaction effects, is also made by means of the Design-Expert 8.0.6 program, and the results are summarized in Table 4. The standardized effects of main effects and interaction effects are the difference between Z_1 and Z_2, where Z_1 and Z_2 are the average response factors at the high and low

Table 4 Standardized effects and contribution of main effects and their two or higher-order interactions

Effect	Standardized effects	Contribution (%)
Main effects		
X_1	−32.04	47.76
X_2	12.95	7.80
X_3	−14.97	10.43
X_4	25.40	30.03
Two–factor interactions		
$X_1 \cdot X_2$	−5.06	1.19
$X_1 \cdot X_3$	6.27	1.83
$X_1 \cdot X_4$	−1.76	0.14
$X_2 \cdot X_3$	−1.31	0.08
$X_2 \cdot X_4$	2.32	0.25
$X_3 \cdot X_4$	1.75	0.14
Three–factor interactions		
$X_1 \cdot X_2 \cdot X_3$	1.36	0.086
$X_1 \cdot X_2 \cdot X_4$	−1.29	0.077
$X_1 \cdot X_3 \cdot X_4$	−1.06	0.052
$X_2 \cdot X_3 \cdot X_4$	1.21	0.068
Four–factor interactions		
$X_1 \cdot X_2 \cdot X_3 \cdot X_4$	1.22	0.069
Lenth's ME	5.25	
Lenth's SME	10.67	

level of the independent variables or their interactions, respectively. A key element in the factorial design statistical procedure is the determination of the significance of the estimated effects. As shown in Table 4, pH of the solution exhibited the highest contribution (47. 76 %) followed by reaction time (30.03 %), Cr(VI) concentration (10.43 %), and loading of catalyst (7.80 %), whereas the interaction effects only accounted for 3.98 % of the total contribution. This suggests the main effects have a direct effect on the Cr (VI) reduction efficiency, whereas the interaction effects on the response factor can almost be ignored.

Another common way to identify the most important effects is to construct the normal probability plot (Box et al. 1978). In such plot, all small effects will appear on a straight line, and any effect with a significant contribution will lie away from the normal probability line. The normal probability plot for the photocatalytic reduction of Cr(VI) is shown in Fig. 5. There are basically six effects lie away from the straight line: in order of significance, pH of the solution, reaction time, Cr(VI) concentration, loading of catalyst, the interaction effects $X_1 \cdot X_3$ and $X_1 \cdot X_2$. These effects are positive indicating that an increase in their level brings about an increase in the photocatalytic reduction efficiency of Cr (VI), while a negative effect indicates an antagonistic effect.

To confirm these results, Pareto chart, a very useful pictorial presentation of the estimated effects and their

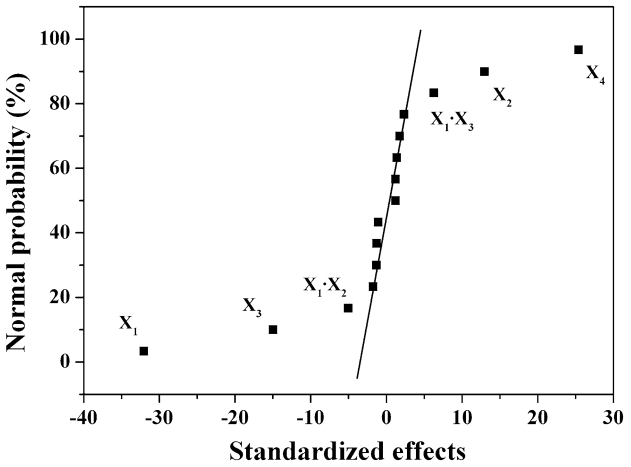

Fig. 5 Normal probability plot of the effects for Cr(VI) reduction efficiency

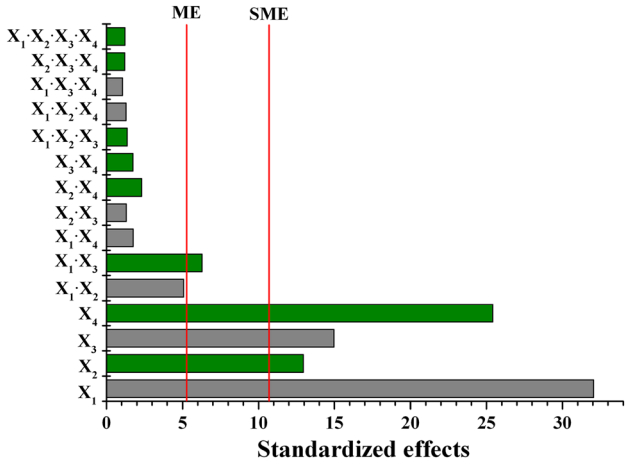

Fig. 6 Pareto chart of the effects for Cr(VI) reduction efficiency for the full 2^4 factorial design. *Olive bars* positive effects; *gray bars* negative effects

statistical importance, is also employed. The Pareto chart displays the absolute values of the effects in a bar chart, as well as the decision lines for a margin of error (ME) and a simultaneous margin of error (SME). The ME and SME values are estimated by the use of Design-Expert 8.0.6 program. All estimated effects greater than the ME, in absolute values, are deemed significant. On the other hand, all other effects whose values are lower than the ME can be attributed to random statistical error. Moreover, an effect that exceeds the ME but lower than SME should be viewed with some caution, as it may be an artifact of testing several effects. In other words, there is at most a 5 % chance that one individual inactive effect will exceed the ME, while there is at most a 5 % chance that any inactive effect will exceed the SME (Zhang et al. 2010). This method offers a simple and fast approach to assess the significance of the main and interaction effects in un-replicated factorial designs.

The Pareto chart of the effects for the photocatalytic reduction efficiency of Cr(VI) is shown in Fig. 6. Four main effects are greater than the SME decision threshold. Among them, the effect of pH and reaction time is much greater than that of Cr(VI) concentration and loading of catalyst. Among the interactions, only the effect of $X_1 \times X_3$ is significant, which needs to be handled with some caution. These results are in good agreement with those shown in Fig. 5. Based on the variables and interactions that are statistically significant, a model describing the experimental response is constructed as follows:

$$Y = 49.05 - 16.02\,X_1 + 6.48\,X_2 - 7.48\,X_3 + 12.70\,X_4 + 3.13\,X_1 \times X_3 \quad (4)$$

where Y is the photocatalytic reduction efficiency of Cr(VI), and X_i are the transformed forms of the independent variables. To ensure the adequacy of the developed model and avoid poor or ambiguous results, an adequate fit of the model should be evaluated (Myers and Montgomery 2002). Analysis of variance (ANOVA) shows the model F value of 90.66 and a very low probability value ((Prob $>$ F) $<$ 0.0001), which confirms that the model is significant for Cr(VI) reduction catalyzed by 25TiO_2/β-FeOOH. The obtained R^2 value and adjusted R^2 are 97.84 and 96.76 %, respectively. Thence, the model developed in this study for predicting Cr(VI) photocatalytic reduction efficiency over 25TiO_2/β-FeOOH was considered to be satisfactory.

Conclusion

The TiO_2/β-FeOOH photocatalysts were successfully synthesized by a simple deposition–precipitation route. The TiO_2 content influenced the photocatalytic activity of the prepared catalysts for Cr(VI) reduction, and the photocatalyst denoted as 25TiO_2/β-FeOOH appeared to be most efficient. The enhanced photocatalytic activity of 25TiO_2/β-FeOOH can be ascribed to effectively inhibiting the recombination of photoinduced electrons and holes, which indicates the possibility of the industrial applications of this photocatalyst for the Cr(VI) reduction. The photocatalytic reduction efficiency of Cr(VI) over 25TiO_2/β-FeOOH was further studied focusing on the influence of operating parameters such as pH of the solution (X_1), loading of catalyst (X_2), Cr(VI) concentration (X_3), and reaction time (X_4) by using a 2^4 factorial design approach. The results obtained from the present study reveal that the main effects (X_1, X_2, X_3, and X_4) and interaction effect of $X_1 \times X_3$ have a significant effect on the Cr(VI) reduction efficiency, whereas the other interaction effects on the response factor can be ignored. ANOVA shows that the developed model in this study for predicting Cr(VI) photocatalytic reduction

efficiency has a high coefficient of determination value ($R^2 = 97.84$ %).

Acknowledgments This work was supported by the National Natural Science Foundation of China (40930738, 21077053). The authors would like to thank Mr. Jianjian Wang for his excellent technical assistance.

References

Banić N, Abramović B, Krstić J, Šojić D, Lončarević D, Cherkezova-Zheleva Z, Guzsvány V (2011) Photodegradation of thiacloprid using Fe/TiO_2 as a heterogeneous photo-Fenton catalyst. Appl Catal B 107:363–371

Barrera-Díaz CE, Lugo-Lugo V, Bilyeu B (2012) A review of chemical, electrochemical and biological methods for aqueous Cr(VI) reduction. J Hazard Mater 223–224:1–12

Benz M, van der Kraan AM, Prins R (1998) Reduction of aromatic nitrocompounds with hydrazine hydrate in the presence of an iron oxide hydroxide catalyst—II. Activity, X-ray diffraction and Mossbauer study of the iron oxide hydroxide catalyst. Appl Catal A 172:149–157

Box GEP, Hunter WG, Hunter JS (1978) Statistics for experimenters. Wiley, New York

Cespón-Romero RM, Yebra-Biurrun MC, Bermejo-Barrera MP (1996) Preconcentration and speciation of chromium by the determination of total chromium and chromium(III) in natural waters by flame atomic absorption spectrometry with a chelating ion-exchange flow injection system. Anal Chim Acta 327:37–45

Cheng ZW, Zhao DN (2011) Effects of experimental conditions on one-dimensional single-crystal nanostructure of β-FeOOH. Mater Chem Phys 127:220–226

Eary LE, Rai D (1988) Chromate removal from aqueous wastes by reduction with ferrous ion. Environ Sci Technol 22:972–977

Eary LE, Rai D (1991) Chromate reduction by subsurface soils under acidic conditions. Soil Sci Soc Am J 55:676–683

Fresno F, Herna'ndez-Alonso MD, David T, Coronado JM, Soria J (2008) Photocatalytic degradation of toluene over doped and coupled (Ti, M)O_2 (M=Sn or Zr) nanocrystalline oxides: influence of the heteroatom distribution on deactivation. Appl Catal B 84:598–606

Jiang F, Zheng Z, Xu ZY, Zheng SR, Guo ZB, Chen LQ (2006) Aqueous Cr(VI) photo-reduction catalyzed by TiO_2 and sulfated TiO_2. J Hazard Mater B134:94–103

Konlen'ko YV, Churagulov BR, Kunst M, Mazerolles L, Colbeau-Justin C (2004) Photocatalytic properties of titania powders prepared by hydrothermal method. Appl Catal B 54:51–58

Ku Y, Jung IL (2001) Photocatalytic reduction of Cr(VI) in aqueous solutions by UV irradiation with the presence of titanium dioxide. Water Res 35:135–142

Li JX, Xu JH, Dai WL, Li HX, Fan KN (2009) Direct hydro-alcohol thermal synthesis of special core–shell structured Fe-doped titania microspheres with extended visible light response and enhanced photoactivity. Appl Catal B 85:162–170

Liang X, Wang X, Zhuang J, Chen YT, Wang DS, Li YD (2006) Synthesis of nearly monodisperse iron oxide and oxyhydroxide nanocrystals. Adv Funct Mater 16:1805–1813

Liu XM, Fu SY, Xiao HM, Huang CJ (2005) Preparation and characterization of shuttle-like α-Fe_2O_3 nanoparticles by supermolecular template. J Solid State Chem 178:2798–2803

Liu LF, Chen F, Yang FL, Chen YS, Crittenden J (2012) Photocatalytic degradation of 2, 4-dichlorophenol using nanoscale Fe/TiO_2. Chem Eng J 181:189–195

Myers RH, Montgomery DC (2002) Response surface methodology: process and product optimization using designed experiments. Wiley, New Jersey

Nriagu J, Nieboer E (1988) Chromium in the natural and human environments. Wiley, New York

Olmez T (2009) The optimization of Cr(VI) reduction and removal by electrocoagulation using response surface methodology. J Hazard Mater 162:1371–1378

Pal B, Sharon M, Nogami G (1999) Preparation and characterization of TiO_2/Fe_2O_3 binary mixed oxides and its photocatalytic properties. Mater Chem Phys 59:254–261

Parida KM, Sahu N (2008) Visible light induced photocatalytic activity of rare earth titania nanocomposites. J Mol Catal A: Chem 287:151–158

Qiu RL, Zhang DD, Diao ZH, Huang XF, He C, Morel JL, Xiong Y (2012) Visible light induced photocatalytic reduction of Cr(VI) over polymer-sensitized TiO_2 and its synergism with phenol oxidation. Water Res 46:2299–2306

Rengaraj S, Venkataraj S, Yeon JW, Kim YH, Li XZ, Pang GKH (2007) Preparation, characterization and application of Nd-TiO_2 photocatalyst for the reduction of Cr(VI) under UV light illumination. Appl Catal B 77:157–165

Ristic M, Music S, Orehovec Z (2005) Thermal decomposition of synthetic ammonium jarosite. J Mol Struct 744:295–300

Singh KP, Singh AK, Gupta S, Sinha S (2011) Optimization of Cr(VI) reduction by zero-valent bimetallic nanoparticles using the response surface modeling approach. Desalin 270:275–284

Štajdohar J, Ristić M, Musić S (2012) Development of porous α-Fe_2O_3 microstructure by forced hydrolysis of $FeCl_3$ solutions in the presence of AOT. J Alloys Compd 532:41–48

Sugimoto T, Muramatsu A (1996) Formation mechanism of monodispersed α-Fe_2O_3 particles in dilute $FeCl_3$ solutions. J Colloid Interface Sci 184:626–638

Sun Q, Leng WH, Li Z, Xu YM (2012) Effect of surface Fe_2O_3 clusters on the photocatalytic activity of TiO_2 for phenol degradation in water. J Hazard Mater 229–230:224–232

Tong GX, Guan JG, Zhang QJ (2011) Goethite hierarchical nanostructures: glucose-assisted synthesis, chemical conversion into hematite with excellent photocatalytic properties. Mater Chem Phys 127:371–378

Wang ZH, Jiang TS, Du YM, Chen KM, Yin HB (2006) Synthesis of mesoporous titania and the photocatalytic activity for decomposition of methyl orange. Mater Lett 60:2493–2496

Xu ZH, Lǔ B, Wu JY, Zhou LX, Lan YQ (2013) Reduction of Cr(VI) facilitated by biogenetic jarosite and analysis of its influencing factors with response surface methodology. Mater Sci Eng C 33:3723–3729

Yoon J, Shim E, Bae S, Joo H (2009) Application of immobilized nanotubular TiO_2 electrode for photocatalytic hydrogen evolution: reduction of hexavalent chromium (Cr(VI)) in water. J Hazard Mater 161:1069–1074

Yu L, Peng XJ, Ni F, Li J, Wang DS, Luan ZK (2013) Arsenite removal from aqueous solutions by γ-Fe_2O_3–TiO_2 magnetic nanoparticles through simultaneous photocatalytic oxidation and adsorption. J Hazard Mater 246–247:10–17

Yuan ZY, Ren TZ, Su BL (2004) Surfactant mediated nanoparticle assembly of catalytic mesoporous crystalline iron oxide materials. Catal Today 93–95:743–750

Yurik TK, Pikaev AK (1999) Radiolysis of weakly acidic and neutral aqueous solutions of hexavalent chromium ions. High Energy Chem 33:208–212

Zhang CY, Wang JL, Zhou HF, Fu DG, Gu ZZ (2010) Anodic treatment of acrylic fiber manufacturing wastewater with boron-doped diamond electrode: a statistical approach. Chem Eng J 161:93–98

Zhao YP, Hu JY, Chen HB (2010) Elimination of estrogen and its estrogenicity by heterogeneous photo-Fenton catalyst beta-FeOOH/resin. J Photochem Photobiol A 212:94–100